American Mineralogist, Volume 68, pages 373–388, 1983

Reversals in Fe–Mg partitioning between chloritoid and staurolite

JEFFREY A. GRAMBLING

Department of Geology
University of New Mexico
Albuquerque, New Mexico 87131

Abstract

Chloritoid and staurolite coexist with Al silicate, chlorite, or garnet ± biotite in Precambrian quartzite and schist from northern New Mexico. Textural and chemical considerations indicate that the minerals crystallized in equilibrium. Chloritoid and staurolite show a reversal in Fe–Mg partitioning: chloritoid consistently is more Fe-rich than staurolite in samples with $X_{Fe,ctd} = 0.95$ to 1.00, but chloritoid is more magnesian than staurolite in samples with $X_{Fe,ctd}$ less than 0.90. Fe–Mg distribution coefficients vary with mineral composition. Linear regression suggests that chloritoid and staurolite should have equal X_{Fe} near 0.909, but only one sample has a composition in that range, and it contains staurolite ($X_{Fe} = 0.93$) coexisting with chloritoid of variable composition ($X_{Fe} = 0.90$ to 0.95). The observed Fe–Mg reversal is not related to variable P, T, or minor element content, including Fe^{3+}. However, it could arise from any of three factors: (1) Fe and Mg may occur on several crystallographic sites in one or both minerals; (2) some Mg may not be exchangeable with Fe in staurolite; or (3) Fe and Mg may mix non-ideally in one or both phases.

Introduction

The distribution of Fe and Mg between coexisting minerals typically varies with temperature but not mineral composition. This permits application of geothermometers based on Fe–Mg partitioning (*e.g.* garnet–biotite or garnet–cordierite: A. B. Thompson, 1976; Holdaway and Lee, 1977; Ferry and Spear, 1978) and suggests that Fe and Mg mix nearly ideally in many silicate minerals (J. B. Thompson, 1957; A. B. Thompson, 1976). If Fe and Mg mix non-ideally in certain minerals, or if Fe and Mg occupy several symmetrically distinct sites in a crystal, then Fe–Mg distribution coefficients could vary with mineral composition and coexisting minerals might show reversals in Fe–Mg partitioning. Reversals would be characterized by changes in distribution coefficients (K_D) across 1.00. Consequences of such reversals are discussed by Korzhinskii (1966) and may include effects associated with extremal states, where reversals coincide with minima or maxima in T–X_{Fe} loops.

There are few well-documented examples of coexisting minerals that show reversals in Fe–Mg partitioning. However, previous studies have suggested that reversals might occur in four systems: biotite–cordierite (Labotka *et al.*, 1981), chloritoid–staurolite (Korikovskii, 1969; Kepezhinskas and Khlestov, 1977), olivine–orthopyroxene, and clinopyroxene–orthopyroxene (Grover and Orville, 1969; Kretz, 1981). In all cases, reversals occur at mineral compositions close to end-member values of Fe/(Fe+Mg). This study addresses the distribution of Fe and Mg in the system chloritoid–staurolite.

Previous work

Coexisting chloritoid and staurolite have been examined by a number of workers. The most comprehensive study is that of Albee (1972), who analyzed the two minerals in samples from 14 localities and found X_{Fe} in chloritoid lower than X_{Fe} in coexisting staurolite in all but two localities. In one of these two places, chloritoid occurs with zincian staurolite and hematite, and Albee (1972, p. 3259) suggested than Zn or Fe^{3+} might cause the anomalous Fe–Mg partitioning. In the second locality showing an apparent Fe–Mg reversal (Albee's area 2), staurolite has a low ZnO content and Albee was unable to account for the reversal. Minerals from this locality have the highest values of Fe/(Fe+Mg) reported by Albee.

Because of Albee's suggestion that ZnO might affect Fe–Mg partitioning, further review is limited to rocks in which staurolite has low ZnO. Five additional papers report compositions of chloritoid coexisting with low zinc staurolite. Three of these (Fox, 1971; Baltatzis, 1979; Lal and Ackermand, 1979) show minerals with X_{Fe} below 0.89, compositions similar to most of Albee's analyses. Chloritoid has lower X_{Fe} than staurolite in these rocks. The remaining two studies (Rumble, 1971; Holdaway, 1978) have minerals with X_{Fe} above 0.92, compositionally similar to minerals in Albee's area 2. Chloritoid in these rocks has X_{Fe} slightly higher than coexisting staurolite.

0003–004X/83/0304–0373$02.00

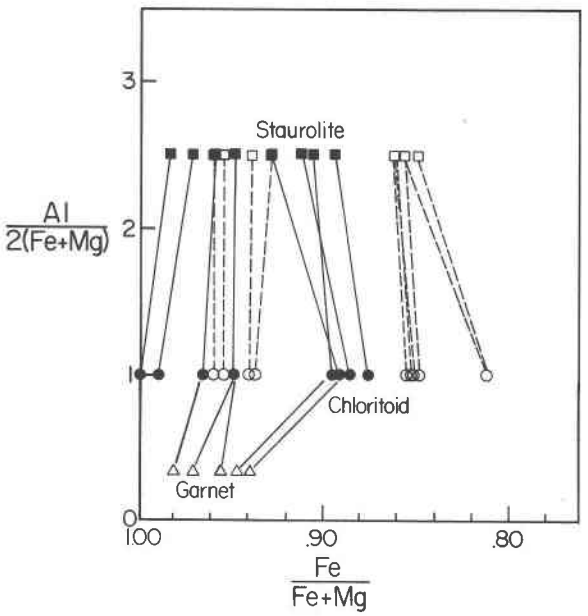

Fig. 1. Chloritoid, staurolite and garnet compositions plotted on an AFM projection (J. B. Thompson, 1957). Dashed lines join minerals reported in studies of Fox (1971), Rumble (1971), Holdaway (1978), Baltatzis (1979) and Lal and Ackermand (1979). Solid tie lines join chloritoid and staurolite from this study. All plotted minerals have less than 1 weight percent ZnO; staurolite is plotted with constant Al_2O_3 to simplify the diagram. Note the reversal in preference for Fe and Mg near $X_{Fe} = 0.91$.

Data from these six studies, summarized together with data from the present study in Figure 1, suggest that staurolite and chloritoid may show a reversal in distribution of Fe and Mg. The published analyses indicate the possibility of an extremal state near $X_{Fe} = 0.90$.

Additional data pertaining to Fe–Mg partitioning between staurolite and chloritoid are presented here, based on analyses of minerals in a suite of Precambrian metamorphic rocks from northern New Mexico. Staurolite and chloritoid are relatively common in the area and range from 0.81 and 1.00 in Fe/(Fe+Mg).

Geologic setting

Most specimens analyzed in this study come from the Truchas Range, located in the southern Sangre de Cristo Mountains, 35 km northeast of Santa Fe, New Mexico (see inset, Fig. 2). Precambrian metamorphic rocks are exposed in a 5 × 10 km block-faulted uplift. Metamorphic rocks include massive crossbedded quartzite, pelitic schist, muscovite schist and amphibolite. These have been folded twice, tightly to isoclinically, with east-trending axes (F_1 and F_2) then gently refolded with northern axes (F_3). Prograde metamorphism overlapped the deformational events, but the present isograd geometry is post-F_2 (Grambling, 1979). The age of metamorphism is estimated to be near 1425 m.y., based on studies of similar rocks in nearby areas (Long, 1972; Gresens, 1975).

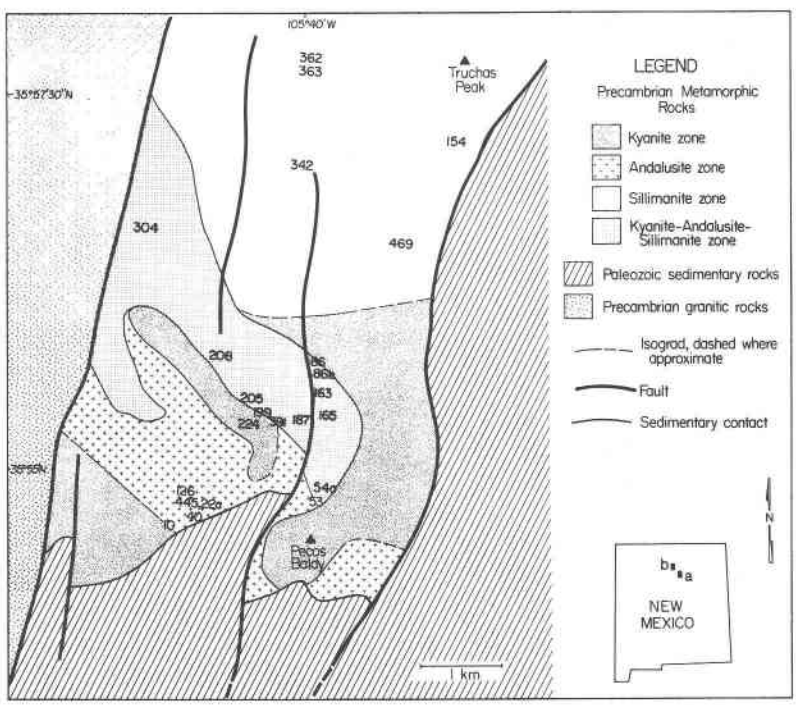

Fig. 2. Metamorphic map of the Truchas Range showing the distribution of Al_2SiO_5 polymorphs, from Grambling (1981). Isograds are controlled mostly by topography. Sample localities are keyed to assemblages in Table 1, but the first two digits are omitted from each station number shown here. Corresponding geologic maps are published in Grambling (1979, 1981).

Grambling (1981) discussed several aspects of metamorphism in the Truchas Range. Kyanite, andalusite and sillimanite coexist across part of the area (Fig. 2), and mineral geothermometry–geobarometry suggests metamorphic conditions near 535°C, 4 kbar. Temperatures and pressures must have varied slightly across the Truchas Range, as indicated by the distribution of Al_2SiO_5 polymorphs, but garnet–biotite geothermometry (Grambling, 1981, this study and unpublished data) indicates that all rocks crystallized in the interval 500–550°C.

Two specimens come from the Picuris Range, New Mexico, 35 km northwest of the Truchas Range, where similar metamorphic rocks are exposed (Montgomery, 1953; Holcombe and Callender, 1982). The Picuris Range may be a faulted extension of the Truchas Range (Montgomery, 1963; Grambling, 1979). Here, also, the three polymorphs of Al_2SiO_5 occur, as well as coexisting chloritoid and staurolite (Holdaway, 1978). According to Holdaway, rocks from the Picuris Range crystallized near 530°C and 3.7 kbar, conditions virtually identical to those in the Truchas Range.

Techniques

Twenty-five specimens of quartsize, pelitic schist and muscovite schist with chloritoid and staurolite, or with closely related mineral assemblages, were collected from the Trunchas Range. Sample localities are indicated in Figure 2. One specimen from the Picuris Range (Pi 45) is from the University of New Mexico collection, exact locality unknown. The other sample from the Picuris Range (P26e) was collected by M. J. Holdaway from the same locality as P26c, described by Holdaway (1978).

Minerals were analyzed using an automated ARL-EMX microprobe at the University of New Mexico, utilizing oxide and silicate standards. Reported analyses represent data from 3 to 4 spots per grain, with several grains of each mineral analyzed in all thin sections. Microprobe data were reduced using a modified Bence–Albee (1968) scheme. Accuracy of reported analyses is estimated as ±3% of the amount present for oxides more abundant than 3 wt.%, ±0.10 wt.% for oxides between 1 and 3 wt.%, and ±0.05 wt.% for oxides less abundant than 1 wt.%. Al and Si have the largest relative errors. These estimates are based on multiple analyses of standards of known composition in the University of New Mexico collection.

Because detection of Fe–Mg reversals is critically dependent on accuracy of the microprobe analyses, additional tests were performed to evaluate analytical accuracy. Chloritoid, staurolite, unzoned garnet and biotite were separated from several samples by crushing the rocks, sieving material to 60–80 mesh, and isolating minerals using magnetic and heavy liquid techniques. Mineral separates were then hand-picked to assure purity in excess of 99 percent and crushed to <200 mesh. Total Fe and Mg were determined for the minerals by atomic absorption spectrophotometry following dissolution in HF, HNO_3 and $HClO_4$ acids. Cesium was added to solutions to eliminate ionization interference, and samples were analyzed in a nitrous oxide-acetylene flame. Comparisons of FeO (total Fe) and MgO analyzed by atomic absorption, to FeO (total Fe) and MgO analyzed by the electron microprobe, are shown in Figure 3: analyses agree to within the error estimates quoted above.

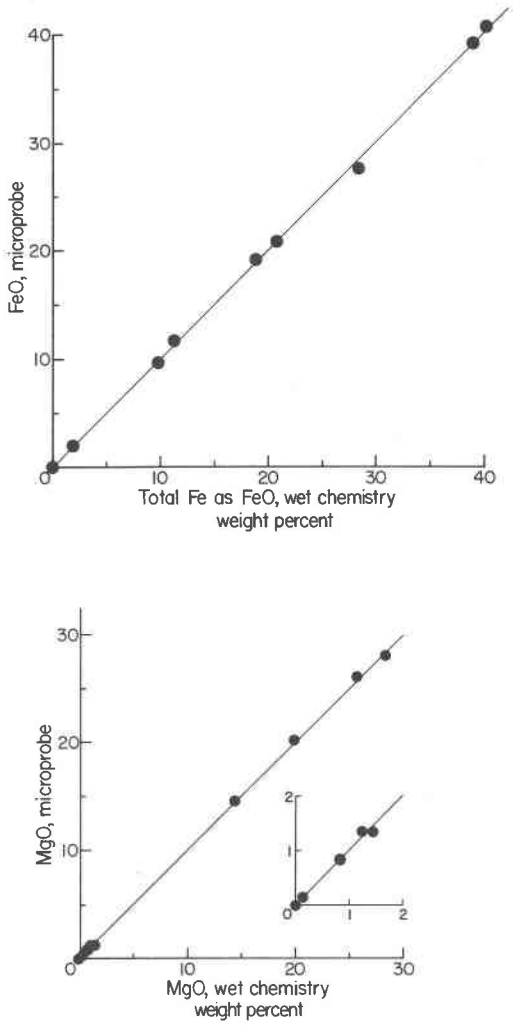

Fig. 3. Comparison of microprobe and wet-chemical analyses for FeO and MgO. Analyses agree to ±3 relative percent for oxides more abundant than 3 weight percent, ±0.10 wt.% for oxides between 1 and 3 wt.%, and ±0.05 wt.% for oxides less abundant than 1 wt.%.

Additionally, ferrous iron determinations were made for several minerals to determine Fe^{3+}/Fe^{2+} ratios. FeO was determined volumetrically by dissolving mineral separates in HF and H_2SO_4 acids, then titrating the solutions with potassium dichromate. Ferric iron was calculated from the difference between FeO and total Fe.

Table 1. Mineral assemblages and FeTi oxide compositions. Sample localities are shown in Figure 2

	Al sil	Biot	Chl	Ctd	Gar	St	Musc	Gra	Rut	Mt	Ilm[1]	Hem[1]
76-391	KAS			x		x	x			x		H(70)I(30)
76-445		x		x	x	x	x	x	x			
76-469	S			x			x					H(75)I(25)
77-10a		2	3	x		x	x		x		I(100)	
77-40-1			x	x		x					H(5)I(95)	
77-53	KAS			x		x	x		x		H(4)I(96)	
77-54a	KAS			x		x	x			x	H(8)I(92)	
77-126		2		x		x	x	x	x		I(100)	
77-154			3	x		x	x					H(65)I(35)
77-163			3	x	x	x	4				H(5)I(95)	
77-165	KAS			x						x		H(74)I(26)
77-187a				x	x	x	x		x		I(100)	
77-199	K			x		x	x					x
77-199b	KS			2			2			x		2
77-205	KA		x			x						x
77-208	KS			x		x	x			x		H(74)I(26)
77-224a				x		x	x		x		H(11)I(89)	
77-304	KS			x			x		x			H(82)I(18)
77-342	KS			x		x	x			x		H(72)I(28)
77-347a	S			3		x	x					H(73)I(27)
77-362	KS			x			x		x			H(68)I(32)
77-363	S			x			x		x			H(81)I(19)
78-22a		x		x	x	x	x		x		H(3)I(96)P(I)	
78-86		x	3		x	x	x		x		H(1)I(99)	
78-86b			3	x	x	x	x			x	H(6)I(94)	
P26e	KA			x		x	x	x	x		x	
Pi 45		x	3	x	x	x	x		x			

[1] Composition reported as mole fraction Fe_2O_3(H) - $FeTiO_3$(I) - $MnTiO_3$(P)

[2] Weathered

[3] Retrograde

[4] Paragonite

Petrography

Chloritoid–staurolite assemblages occur in quartzite, pelitic schist and muscovite schist. Coexisting minerals include aluminum silicate, biotite±garnet, or chlorite. Most specimens contain muscovite, all include quartz, and nearly all have some Fe or Ti oxide phase. Mineral assemblages are listed in Table 1.

Chloritoid forms subhedral to euhedral crystals generally less than 0.3 mm in maximum dimension. In some rocks chloritoid lies parallel to S_1 foliation, but typically it cuts across the S_1 and S_2 fabrics. Crystals tend to have two distinct habits. Several samples contain acicular chloritoid with a pale blue to colorless pleochroism, rare simple twinning on (001), and low first-order interference colors. Other specimens have stubby, near-equidimensional or rarely acicular chloritoid showing intense pleochroism, with pleochroic formula X = green, Y = blue, Z = greenish yellow. These tend to show abundant lamellar twinning on (001). There are no detectable compositional differences between the two varieties of chloritoid, and both can have identical X_{Fe}, but both textural varieties never occur in the same sample.

Staurolite typically forms euhedral porphyroblasts up to 1 cm in length, cutting across the S_1 and S_2 fabrics. Staurolite and chloritoid appear in mutual contact in most rocks and are separated by only a few millimeters in the rest. The two minerals do not show obvious reaction textures except in specimen 77-54a, where intergrowths of chloritoid and sillimanite form partial pseudomorphs after staurolite, and in specimen 77-347a, where some chloritoid occurs in fractures cutting across staurolite and fibrolitic sillimanite. The textures of 77-347a may indicate retrograde growth of chloritoid, so that sample is not considered further.

Chlorite is a retrograde mineral in many samples (Table 1). It is typically present in trace amounts, cuts across foliation and seems to have grown at the expense of preexisting biotite or rarely garnet. Prograde chlorite occurs in only two specimens, 77-40-1 and 77-205, where it is aligned parallel to S_1 foliation and is strained or kink-banded. Chlorite must be older than regional deformation in these two samples. Peak metamorphism occurred after regional deformation, justifying the interpretation that these chlorites are prograde (*cf.* Grambling, 1981).

Table 2. Microprobe analyses of biotite, muscovite and paragonite

	Biotite				Muscovite					
	76-445	77-126[1]	78-22a	78-86	76-445	77-163[2]	77-205	78-22a	78-86	78-86b
	weight percent oxide									
FeO	26.00	20.75	25.63	25.23	.90	.63	1.46	1.10	1.25	1.26
MgO	5.89	5.46	6.13	6.35	.31	.06	.67	.27	.49	.39
MnO	.01	.07	.02	.03	.00	.00	.01	.00	.00	.00
TiO_2	1.53	.86	1.38	1.54	.12	.08	.21	.12	.24	.25
Al_2O_3	19.96	22.74	20.39	20.56	35.62	39.75	37.19	37.43	36.82	37.03
SiO_2	33.41	37.67	34.16	33.95	46.24	45.20	47.79	46.68	46.90	46.73
K_2O	7.49	5.83	7.31	8.32	9.28	.96	7.70	8.79	6.84	7.10
Na_2O	.13	.10	.19	.24	.93	6.88	1.65	.81	1.96	2.05
CaO	.03	.02	.05	.00	.01	.06	.00	.00	.00	.00
Total	94.45	93.50	95.26	96.22	93.41	94.31	96.68	95.20	94.52	94.81
	cations based on 11 oxygens									
Fe	1.71	1.31	1.66	1.63	.05	.03	.08	.06	.07	.07
Mg	.69	.61	.71	.73	.03	.05	.06	.03	.05	.04
Mn	.00	.00	.00	.00	.00	.00	.00	.00	.00	.00
Ti	.09	.05	.08	.09	.01	.01	.01	.01	.01	.01
Al	1.85	2.02	1.86	1.87	2.82	3.03	2.83	2.90	2.85	2.87
Si	2.63	2.83	2.65	2.62	3.11	2.97	3.09	3.07	3.08	3.07
K	.75	.56	.72	.82	.80	.08	.63	.74	.57	.59
Na	.02	.01	.03	.04	.12	.86	.21	.10	.25	.26
Ca	.00	.00	.00	.00	.00	.00	.00	.00	.00	.00
$\frac{Fe}{Fe + Mg}$	.71	.68	.70	.69	$\frac{K}{K + Na}$ .87	.08	.75	.88	.70	.69

[1] altered

[2] paragonite

Mineralogy

Aluminum silicate minerals include kyanite, andalusite and sillimanite. These are nearly pure Al_2SiO_5 with minor Fe_2O_3 (0.05–1.70 wt.%), less than 0.04 wt.% MgO and less than 0.01 wt.% TiO_2. As discussed by Grambling (1981), andalusite consistently has higher Fe_2O_3 than kyanite and sillimanite, which have similar Fe_2O_3 contents.

Biotite has ratios Fe/(Fe+Mg) from 0.68 to 0.71 with less than 1.55 wt.% TiO_2, 0.07 wt.% MnO, 0.25 wt.% Na_2O and 0.05 wt.% CaO (Table 2). Biotite shows substitutions of the type $(Fe,Mg)^{VI} + Si^{IV} = 2Al$ and is typically slightly deficient in alkalis. Biotite is fresh in all samples except 77-10a and 77-126 where it is partially altered to a greenish mineral, possibly vermiculite.

Muscovite is principally composed of $KAl_3Si_3O_{10}(OH)_2$ and $NaAl_3Si_3O_{10}(OH)_2$ (Table 2). It shows minor deficiencies in alkalis, up to 2.1 wt.% (FeO+MgO) and up to 0.25 wt.% TiO_2. Muscovite has less than 31 mole percent paragonite in solid solution. Primary paragonite occurs in specimen 77-163 and contains 8 mole percent of the muscovite molecule, but no rocks with muscovite and paragonite have been recognized among those listed in Table 1.

Chlorite occurs in several specimens and consists chiefly of solid solution between $Fe_{4.5}Al_3Si_{2.5}O_{10}(OH)_8$ and $Mg_{4.5}Al_3Si_{2.5}O_{10}(OH)_8$ (Table 3). Chlorite typically has trace amounts of MnO and TiO_2 and is retrograde in most samples in which it occurs (Table 1).

Garnet consists of solid solution of almandine, pyrope and spessartine with minor grossular. Trace amounts of TiO_2 have been detected in garnet from several rocks, and garnet contains 0.60 wt.% Fe_2O_3 in specimen 78-86b (analyzed by wet chemistry). Garnet is unzoned in all samples listed in Table 3, although zoned garnets are common in rocks lacking chloritoid + staurolite in the area.

Chloritoid consists of $Fe_2Al_4Si_2O_{10}(OH)_4$ to $Mg_2Al_4Si_2O_{10}(OH)_4$ (Table 4). Most crystals have minor amounts of ZnO (up to 0.28 wt.%), TiO_2 (up to 0.68 wt.% and MnO (up to 2.83 wt.%). Chloritoid crystals have no compositional zoning with the notable exception of specimen P26e, where all grains are zoned. In P26e, individual

Table 3. Microprobe analyses of garnet and chlorite. Garnet rim compositions are reported, although all garnets are essentially unzoned.

	Garnet rim						Chlorite				
	76-445	77-163	77-187a	78-22a	78-86	78-86b	77-40-1	77-163[1]	77-205	78-86[1]	78-86b[1]
	weight percent oxide										
FeO	36.98	42.28	41.34	41.24	40.64	41.19	30.23	39.13	13.42	34.50	39.09
MgO	1.36	.68	.53	1.37	1.47	1.35	8.64	3.09	21.19	7.60	4.47
MnO	4.32	.31	.41	.18	.18	.20	.10	.05	.14	.00	.01
CaO	.61	.18	.22	.28	.32	.34	.00	.00	.00	.00	.00
TiO_2	.03	.00	.06	.00	.03	.00	.07	.02	.01	.08	.07
Al_2O_3	21.13	20.79	21.07	20.68	20.71	20.84	24.68	22.84	23.55	22.11	22.15
SiO_2	36.57	36.36	36.41	36.24	36.74	36.68	25.60	21.22	26.67	22.45	22.14
Total	101.00	100.60	100.04	99.99	100.09	100.60	89.32	86.35	84.98	86.74	87.93
	cations based on 12 oxygens, garnet; 14 oxygens, chlorite										
Fe	2.51	2.90	2.84	2.83	2.78	2.81	2.66	3.81	1.12	3.25	3.72
Mg	.16	.08	.06	.17	.18	.16	1.35	.54	3.24	1.28	.76
Mn	.30	.02	.03	.01	.01	.01	.01	.00	.01	.00	.00
Ca	.05	.02	.02	.02	.03	.03	.00	.00	.00	.00	.00
Ti	.00	.00	.00	.00	.00	.00	.01	.00	.00	.01	.01
Al	2.02	2.01	2.04	2.00	2.00	2.00	3.06	3.13	2.79	2.94	2.97
Si	2.97	2.98	2.99	2.98	3.00	2.99	2.69	2.47	2.68	2.53	2.52
$\frac{Fe}{Fe + Mg}$	.94	.97	.98	.94	.94	.95	.66	.88	.26	.72	.83

[1] retrograde

chloritoid crystals vary in composition from $X_{Fe} = 0.90$ to $X_{Fe} = 0.95$, with single grains zoned across the entire compositional range. There is no apparent pattern to the zoning: some crystals have high-Mg cores and zone outward to low-Mg rims; other crystals have low-Mg cores and zone outward to high-Mg rims; other crystals show irregular zoning patterns (Fig. 4). Analyses of edges of chloritoid grains in P26e vary across the entire compositional range, from 0.7 to 2.3 weight percent MgO. A histogram (see inset, Fig. 4) shows that most chloritoid edge analyses in P26e fall near 0.8 wt.% MgO ($X_{Fe} = 0.95$). Interpretations of these unusual zoning profiles are discussed in a following section.

X-ray diffraction analysis of chloritoid in sample 78-86b shows the mineral to be the triclinic polymorph (Halferdahl, 1961). No other samples contained enough chloritoid to obtain a separate for X-ray work.

Staurolite is primarily a solid solution of four components, $Fe_4Al_{18}Si_8O_{48}H_2$, $Mg_4Al_{18}Si_8O_{48}H_2$, $Zn_4Al_{18}Si_8O_{48}H_2$ and $Mn_4Al_{18}Si_8O_{48}H_2$ (Table 5; *cf.* Smith, 1968; Hollister, 1970; Griffen and Ribbe, 1973). Analyzed crystals have up to 5.76 wt.% ZnO and 1.08 wt.% MnO, although most are close to binary Fe–Mg solutions. All have TiO_2 content less than 0.54 wt.%. Most crystals are deficient in Si relative to the idealized formula, with cations Si ranging from 7.44 to 7.91 per 47 oxygens, averaging 7.77. Staurolite has excess Al relative to the ideal formula, with Al varying from 17.98 to 18.84 cations per 47 oxygens; the more aluminous grains have Al content close to the maximum reported for staurolite (*cf.* Griffen and Ribbe, 1973; Hollister, 1970, sector (001)). Staurolite is unzoned in all specimens except 76-445, where Fe/(Fe+Mg) increases from 0.90 or 0.91 in the center of grains to 0.94 at crystal edges.

Rutile and magnetite form subhedral to euhedral crystals that are essentially pure TiO_2 and Fe_3O_4, respectively. Hematite ranges in composition from $Hem_{65}Ilm_{35}$ to $Hem_{82}Ilm_{18}$, and ilmenite varies from $Hem_{11}Ilm_{89}$ to pure $FeTiO_3$ according to broad-beam microprobe analyses (Table 1). Ilmenite rarely has minor amounts of MnO, ranging up to the equivalent of 1 mole percent $MnTiO_3$ in sample 78-22a. No primary hematite–ilmenite pairs occur in any rocks considered in this study, although ilmenite has exsolved as fine lamellae in numerous hematite crystals, and magnetite is partly converted to pure Fe_2O_3 in sample 77-54a, presumably a result of supergene alteration.

Elemental partitioning

Twelve samples from Table 1 contain chloritoid and staurolite with MnO + ZnO less than 1 wt.%. Two of these show significant signs of weathering (77-10a, 77-

Table 4. Microprobe analyses of chloritoid

	Chloritoid													
	76-391	76-445	76-469	76-10a	77-40-1	77-53	77-54a	77-126	77-154	77-163	77-165	77-187a	77-199	77-199b
FeO	28.67	25.95	27.61	26.07	25.81	25.67	28.82	25.61	24.45	28.17	27.65	26.98	25.99	28.11
MgO	.16	1.79	.48	1.78	1.87	2.03	.01	1.69	1.55	.77	.39	.56	.53	.08
MnO	.28	.17	.33	.34	.21	.39	.19	.36	1.32	.02	.35	.05	.33	.46
ZnO	.02	.04	.08	.01	.00	.07	.01	.00	.19	.01	.28	.15	.00	.22
TiO_2	.04	.00	.01	.03	.00	.01	.68	.12	.00	.01	.02	.01	.00	.01
Al_2O_3	39.97	40.83	39.88	40.93	40.71	40.76	39.57	40.21	40.15	39.50	40.55	39.90	41.04	39.47
SiO_2	23.77	24.28	23.63	24.08	24.17	24.34	24.14	23.87	24.06	23.91	23.90	23.55	24.60	23.59
Total	92.91	93.06	92.02	93.24	92.77	93.27	93.42	91.86	91.72	92.39	93.14	91.36	92.49	91.94
	cations based on 12 oxygens													
Fe	2.02	1.79	1.95	1.80	1.79	1.77	2.01	1.79	1.71	1.99	1.93	1.92	1.80	2.00
Mg	.02	.22	.06	.22	.23	.25	.00	.21	.19	.10	.05	.07	.07	.01
Mn	.02	.01	.02	.02	.01	.03	.01	.03	.09	.00	.02	.00	.02	.03
Zn	.00	.00	.00	.00	.00	.00	.00	.00	.01	.00	.02	.01	.00	.01
Ti	.00	.00	.00	.00	.00	.00	.04	.01	.00	.00	.00	.00	.00	.00
Al	3.96	3.98	3.97	3.98	3.98	3.96	3.90	3.97	3.97	3.92	3.99	3.99	4.02	3.96
Si	2.00	2.01	2.00	1.99	2.00	2.01	2.02	2.00	2.02	2.01	2.00	2.00	2.04	2.01
$\frac{Fe}{Fe+Mg}$	.99	.89	.97	.89	.89	.88	1.00	.89	.90	.95	.98	.97	.96	.99

	Chloritoid											
	77-208	77-224a	77-304	77-342	77-347a	77-362	77-363	78-22a	78-86b	P26e high Mg	P26e low Mg	P145
FeO	28.43	27.56	26.09	27.13	28.39	25.40	26.23	25.33	27.56	25.79	26.60	25.06
MgO	.39	.84	.70	.49	.04	.76	.84	1.64	.81	1.52	.72	1.99
MnO	.39	.03	2.36	1.64	.64	2.83	1.38	.26	.01	.19	.24	.42
ZnO	.28	.01	.31	.28	.07	.08	.14	.00	.00	.18	.18	.28
TiO_2	.02	.01	.00	.01	.07	.03	.15	.00	.00	.01	.01	.01
Al_2O_3	39.17	39.92	40.07	40.33	40.24	39.30	39.96	40.48	40.14	40.35	39.67	41.49
SiO_2	23.86	23.75	23.23	23.39	24.24	24.21	23.95	23.88	23.62	23.63	23.51	23.69
Total	92.54	92.12	92.76	93.27	93.66	92.61	92.65	91.59	92.14	91.67	90.93	92.94
	cations based on 12 oxygens											
Fe	2.01	1.94	1.84	1.90	1.98	1.79	1.84	1.78	1.94	1.81	1.90	1.73
Mg	.05	.11	.09	.06	.00	.10	.10	.20	.10	.19	.09	.25
Mn	.03	.00	.17	.12	.05	.20	.10	.02	.00	.01	.02	.03
Zn	.02	.00	.02	.02	.00	.00	.01	.00	.00	.01	.01	.02
Ti	.00	.00	.00	.00	.00	.00	.01	.00	.00	.00	.00	.00
Al	3.90	3.96	3.98	3.99	3.95	3.89	3.95	4.00	3.99	4.00	3.98	4.04
Si	2.02	2.00	1.96	1.96	2.02	2.03	2.01	2.00	1.99	1.99	2.00	1.96
$\frac{Fe}{Fe+Mg}$	.98	.95	.95	.97	1.00	.95	.95	.90	.95	.90	.95	.88

126: see Table 1) so are omitted from the following discussion. The remaining 10 have Fe/(Fe+Mg) in chloritoid ranging from 1.00 to 0.88 and in staurolite from 0.97 to 0.89.

Tie lines showing relative Fe/(Fe+Mg) of coexisting chloritoid and staurolite appear in Figure 1. Staurolite compositions plot across the entire range in X_{Fe}. With the exception of sample P26e, chloritoid analyses show a distinct gap, with no analyzed crystals having X_{Fe} between 0.90 and 0.95. Chloritoid in P26e has variable composition, with analyses falling within the range X_{Fe} = 0.90 to 0.95. Tie lines indicate the presence of a reversal in Fe–Mg partitioning: for mineral pairs with high X_{Fe}, chloritoid has higher X_{Fe} than staurolite; but for mineral pairs with low X_{Fe}, staurolite has higher X_{Fe} than chloritoid. The data are virtually identical to those from previous studies and indicate an Fe–Mg reversal for the two minerals at X_{Fe} between 0.90 to 0.95.

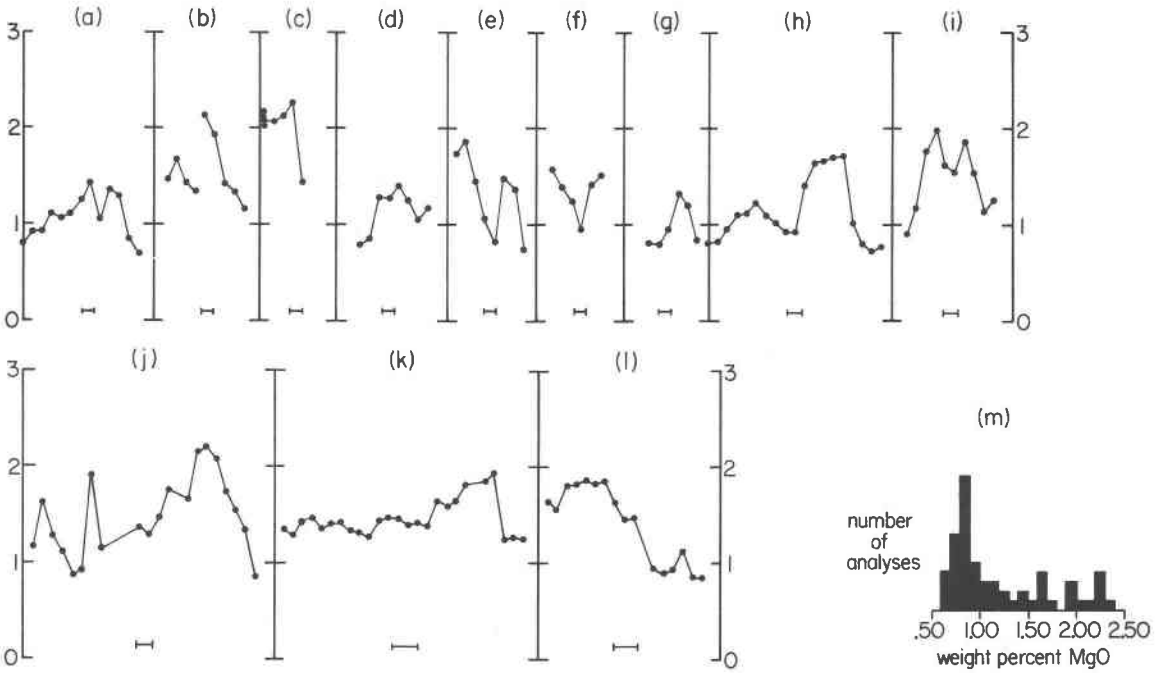

Fig. 4. Microprobe traverses across 12 individual chloritoid crystals in specimen P26e, showing variation in weight percent MgO. Scale bar in each figure is 5μ in length. Analytical precision for high-Mg analyses is ±0.08 wt.% MgO, as indicated by replicate analyses in traverse c. Inset m shows histogram of edge analyses (n = 63).

Korikovskii (1969, Fig. 3) presents data suggesting an Fe–Mg reversal between chloritoid and garnet near X_{Fe} = 0.93. Data in the present study do not confirm this second reversal. Chloritoid is uniformly lower in X_{Fe} than coexisting garnet in five samples with $X_{Fe,ctd}$ ranging from 0.89 to 0.97 (Fig. 1).

Differences in X_{Fe} between coexisting chloritoid and staurolite are generally larger than maximum expected errors in microprobe analyses (±0.006 in X_{Fe} for each mineral). Furthermore, the differences shown in Figure 1 are systematically related to mineral compositions, and Figure 3 shows no systematic errors in FeO or MgO determinations. Therefore the Fe–Mg reversals cannot be attributed to inaccurate analyses. However, three other interpretations could fit the data: (1) mineral compositions do not represent equilibrium; (2) minor elements, possibly Fe^{3+}, are perturbing the data, and reversals do not occur in the system Fe^{2+}–Mg; or (3) the reversals are a real factor of equilibrium phase relations in natural chloritoid and staurolite.

Analysis of equilibrium

Mineral textures are consistent with equilibrium with the exceptions of chlorite in several samples and chloritoid in specimen 77-347a. Minerals show no reaction textures and typically occur in mutual contact. Mineral compositions are constant on the scale of a thin section, even for zoned minerals such as staurolite in 76-445, if only edge compositions are considered. The sole exception is chloritoid in P26e. Two samples (77-163, 78-86b) have inclusions of chloritoid + staurolite in garnet. Included minerals show the same sense of Fe–Mg partitioning as matrix phases. Because garnet serves to isolate inclusions from reaction or chemical exchange with matrix minerals (Hollister, 1969; Tracy *et al.*, 1976, p. 771; Rumble, 1978, p. 329), it seems unlikely that the composition of either phase was altered after its crystallization, hence it is unlikely that the Fe–Mg reversals are due to partial retrogression.

Biotite–garnet pairs occur in three samples (76-445, 78-22a, 78-86) and show values of K_D (Fe–Mg) of 6.33, 7.12 and 6.92, respectively. These indicate temperatures of 500–535°C according to the calibration of Ferry and Spear (1978), similar to regional metamorphic temperatures calculated by Grambling (1981) using several different geothermometers. This suggests that biotite and garnet preserve Fe/Mg ratios representative of peak metamorphic conditions, and it indirectly supports the contention that chloritoid and staurolite should do the same.

Figure 5 shows compositions of FeTi oxide minerals plotted on the plane FeO–Fe_2O_3–TiO_2. The lack of crossing tie lines suggests that the oxide minerals attained chemical equilibrium. However, the AFM projection (J. B. Thompson, 1957) shows four-phase assemblages and several crossing tie lines (Fig. 6). This could be due to (1) retrograde effects; (2) failure of the projection to represent minor elements such as ZnO, MnO or Fe_2O_3; or (3) failure of mineral assemblages to satisfy conditions under

Table 5. Microprobe analyses of staurolite

	Staurolite													
	76-391	76-445[1]	77-10a	77-40-1	77-53	77-54a	77-126	77-154	77-163	77-187a	77-205	77-208	77-224a	77-342
	weight percent oxide													
FeO	12.02	14.83	14.74	13.75	13.45	13.09	14.54	8.56	14.94	15.54	8.21	10.12	14.11	8.65
MgO	.20	.65	1.00	.74	.90	.13	1.13	.54	.95	.39	1.21	.83	.44	1.10
MnO	.42	.09	.13	.09	.21	.23	.24	.51	.01	.02	.19	.33	.03	1.08
ZnO	.49	.00	.05	.39	.11	.17	.32	5.76	1.09	.20	1.50	4.34	.00	4.67
TiO_2	.37	.48	.34	.38	.52	.50	.34	.37	.54	.50	.39	.22	.44	.27
Al_2O_3	56.21	55.14	54.73	55.61	55.72	56.33	53.63	55.46	53.31	53.83	57.22	54.50	55.55	56.16
SiO_2	27.51	27.61	28.19	28.36	26.69	26.95	27.80	27.08	26.84	27.21	28.30	27.88	27.49	26.18
Total	97.22	98.80	99.18	99.32	97.60	97.40	98.00	98.28	97.68	97.69	97.02	98.22	98.06	98.11
	cations based on 47 oxygens													
Fe	2.85	3.49	3.46	3.21	3.19	3.10	3.46	2.03	3.59	3.72	1.92	2.40	3.33	2.06
Mg	.08	.27	.42	.31	.38	.05	.48	.23	.41	.17	.50	.35	.19	.47
Mn	.10	.02	.03	.02	.05	.06	.06	.12	.00	.00	.04	.08	.01	.26
Zn	.10	.00	.01	.08	.02	.04	.07	1.21	.23	.04	.31	.91	.00	.98
Ti	.08	.10	.07	.08	.11	.11	.07	.08	.12	.11	.08	.05	.09	.06
Al	18.76	18.31	18.09	18.28	18.65	18.83	17.98	18.57	18.07	18.18	18.84	18.23	18.50	18.82
Si	7.79	7.78	7.90	7.91	7.58	7.64	7.91	7.69	7.72	7.79	7.90	7.91	7.77	7.44
$\frac{Fe}{Fe+Mg}$	.97	.93	.89	.91	.89	.98	.88	.90	.90	.96	.79	.87	.95	.82

	Staurolite					
	77-347a	78-22a	78-86	78-86b	P26e	Pi45
	weight percent oxide					
FeO	9.18	14.36	14.48	12.70	13.60	14.65
MgO	1.20	.86	.72	.44	.56	1.14
MnO	.95	.07	.00	.00	.06	.20
ZnO	4.84	.00	.67	2.55	.19	.54
TiO_2	.38	.46	.38	.38	.45	.54
Al_2O_3	53.98	54.22	53.76	54.29	55.59	54.76
SiO_2	27.63	27.23	26.85	26.50	27.76	26.63
Total	98.16	97.20	96.86	96.86	98.21	98.46
	cations based on 47 oxygens					
Fe	2.19	3.43	3.49	3.07	3.20	3.48
Mg	.51	.37	.31	.19	.24	.48
Mn	.23	.02	.00	.00	.01	.05
Zn	1.02	.00	.14	.54	.04	.11
Ti	.08	.10	.08	.08	.10	.12
Al	18.11	18.28	18.27	18.48	18.46	18.34
Si	7.86	7.79	7.74	7.65	7.82	7.57
$\frac{Fe}{Fe+Mg}$	.81	.90	.92	.94	.93	.88

[1]Zoned to higher X_{Fe} at edge; edge analysis given

which the AFM diagram behaves as a valid phase projection (J. B. Thompson, 1957; Greenwood, 1975; Rumble, 1978). The first explanation is not supported by mineral textures, because no chlorite-bearing rocks are plotted in Figure 6, nor is specimen 77-347a with texturally retrograde chloritoid. The second explanation also seems inconsistent with the data. All minerals plotted in Figure 6 have MnO + ZnO contents less than 1 wt.%, and the silicate minerals have low Fe_2O_3 contents (see following section). Tie lines cross for assemblages that crystallized at equal $f(O_2)$, as indicated by nearly constant $X(Fe_2O_3)$ in hematite that coexists with magnetite, also suggesting that variable Fe^{3+} does not control the crossing tie lines.

The AFM projection will behave as an equilibrium

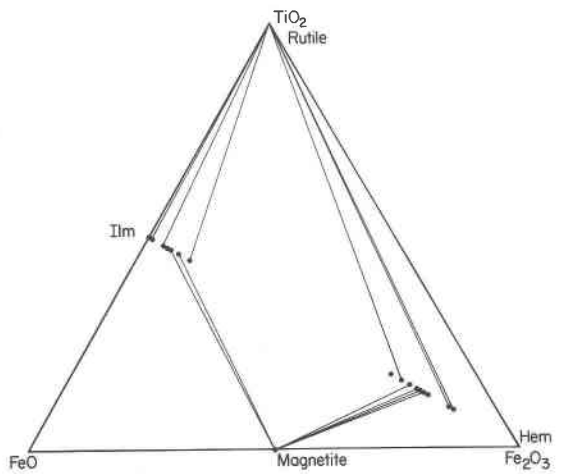

Fig. 5. FeTi oxide minerals plotted on plane FeO–Fe_2O_3–TiO_2.

phase diagram only if all rocks crystallized at equal values of P, T and $\mu(H_2O)$. The presence of coexisting kyanite, andalusite and sillimanite, as well as biotite–garnet geothermometry, provides evidence that all rocks crystallized at about the same P and T (see also Grambling, 1981, p. 708). However, the possibility that the rocks crystallized at variable $\mu(H_2O)$ must be evaluated separately. Such evaluation can be done by projecting mineral compositions onto a plane that includes H_2O. There are not enough minerals of fixed composition for rigorous application of the projection techniques of J. B. Thompson (1957) or Greenwood (1975), but staurolite occurs in most rocks and has a fairly limited compositional range (X_{Fe} = 0.88 to 0.98, excluding crystals rich in ZnO). A projection from staurolite (assuming X_{Fe} = 0.90), muscovite and quartz onto the plane FeO–MgO–H_2O appears in Figure 7 (*cf.* Rumble, 1978, Fig. 7). All crossing tie lines are eliminated except for a slight crossing of the biotite–chloritoid tie in one pair of samples, and a slight crossing of the chloritoid–staurolite tie in another sample (note that staurolite does not plot in Fig. 7). The differences in X_{Fe} that cause these ties to cross are within the range of expected analytical error. Therefore the projection seems to work satisfactorily as a phase diagram, suggesting that the rocks crystallized at variable $\mu(H_2O)$, and further suggesting that minerals preserve their equilibrium compositions.

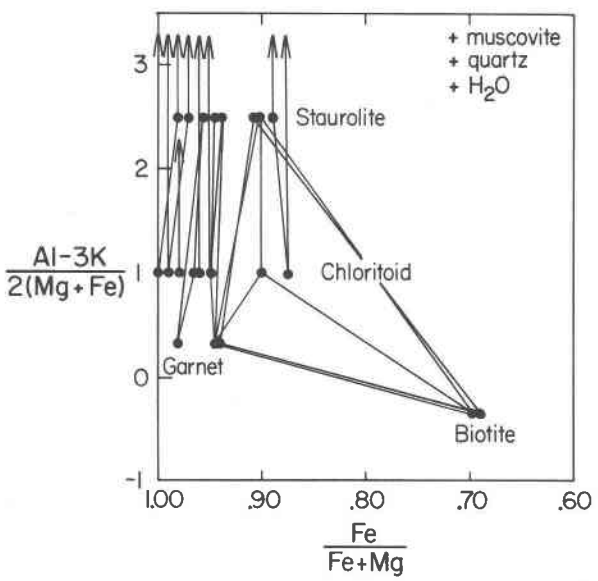

Fig. 6. AFM projections (J. B. Thompson, 1957) showing mineral assemblages in the Truchas Range. All plotted phases have ZnO + MnO less than 1 weight percent, and no texturally retrograde minerals are shown. See text for discussion of crossing tie lines.

Effects of Mn, Zn and Fe^{3+}

The minor elements Zn and Mn exert a substantial effect on Fe/(Fe+Mg) ratios of staurolite and chloritoid. This is displayed graphically in Figure 8: in the assemblage chloritoid–staurolite–Al silicate–muscovite–quartz, the ratio Fe/(Fe+Mg) decreases by 18 mole percent in staurolite, and by 3 mole percent in chloritoid, as the amount of ZnO in staurolite increases from 0.17 to 4.67 wt.%. However, this effect is not responsible for the observed Fe–Mg reversal, because values of K_D (Fe–Mg) vary only from 0.02 to 0.35 for samples shown in Figure 8. The Fe–Mg reversal occurs in minerals with low ZnO+MnO contents (Fig. 1), and Figure 9 demonstrates that there is no relationship between K_D and Zn+Mn content.

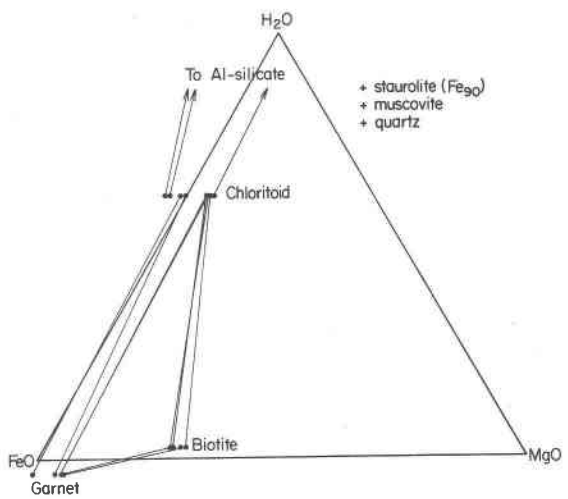

Fig. 7. Mineral assemblages projected onto the plane FeO–MgO–H_2O. Minerals are projected from muscovite, quartz and staurolite (X_{Fe} = 0.90) using the projection technique of Greenwood (1975).

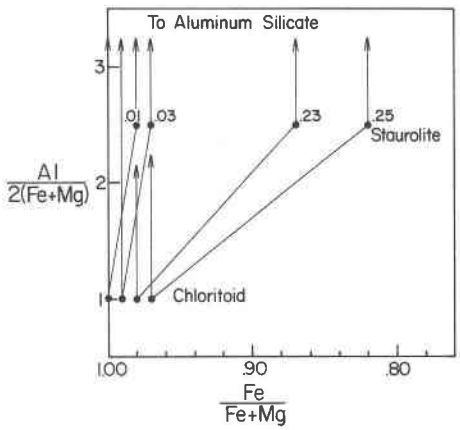

Fig. 8. AFM projection (J. B. Thompson, 1957) showing mineral compositions in specimens 77-54a, 76-391, 77-208 and 77-342. Numbers by staurolite represent $X_{Zn,st}$ and illustrate how X_{Fe} varies with X_{Zn} in staurolite for the assemblage chloritoid–staurolite–Al silicate.

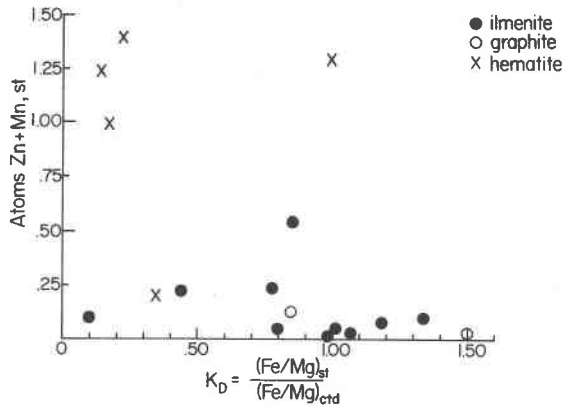

Fig. 9. Plot of staurolite minor element content against K_D (Fe–Mg, st-ctd). Symbols are keyed to oxide assemblage in each sample.

Ferric iron is not determined by microprobe analyses but might be responsible for the apparent Fe–Mg reversal. If Fe^{3+}/Fe^{2+} were high in chloritoid but low in staurolite, then Fe^{2+}/Mg ratios might not show the reversal that is indicated by total Fe/Mg. Chloritoid is a volumetrically minor phase in most samples, making it difficult to separate in quantities large enough for accurate Fe^{3+} analysis. Only one specimen (78-86b) contained enough chloritoid to obtain a useful mineral separate. Multiple wet chemical analyses indicate that this chloritoid has 5 to 8 percent of its total Fe as Fe^{3+}. This shifts $Fe^{2+}/(Fe^{2+}+Mg)$ by only 0.003 relative to total Fe/(Fe+Mg). Even assuming no Fe^{3+} in staurolite, a shift of 0.003 in X_{Fe} in chloritoid is not enough to reverse the observed Fe–Mg distribution in that sample.

This result can be generalized to other samples by assuming that silicate and oxide minerals crystallized in equilibrium. Specimen 78-86b contains ilmenite with 6 mole% Fe_2O_3 in solid solution. Seven other samples contain ilmenite with less than 6 mole% Fe_2O_3; chloritoid in these samples should have similar or lower Fe^{3+} content than chloritoid in 78-86b. These eight samples show a reversal in Fe–Mg distribution (Fig. 9), with differences in Fe/(Fe+Mg) between staurolite and chloritoid considerably larger than 0.003 in most specimens. Therefore it appears that Fe^{3+} is not responsible for the observed Fe–Mg reversal.

Because the Fe–Mg reversal cannot be related to analytical errors, disequilibrium, Mn, Zn, or Fe^{3+} content, it is likely that the reversal is part of the equilibrium phase relations between natural chloritoid and staurolite.

Compositional relationships

The distribution coefficient between chloritoid and staurolite varies as a linear function of mineral Fe/(Fe+Mg) ratios. This is illustrated in Figure 10 using data from the Truchas Range, including zincian samples, where the relationship can be expressed as $K_D = -9.38 X_{Fe,ctd} + 9.53$, with $r^2 = 0.74$ (standard error of estimate = 0.05; Alder and Roessler, 1972, p. 205). Data from other areas (Fig. 1) fall along the same trend. Two items are noteworthy: (1) The least squares line crosses $K_D = 1.00$ at $X_{Fe,ctd} = 0.909 \pm .019$. This agrees well with the composition of the chloritoid–staurolite reversal inferred from data in previous studies, 0.90 (Fig. 1). (2) There is a gap in chloritoid compositions from $X_{Fe} = 0.90$ to 0.95 in all samples but P26e. Sample P26e displays unusual zoning that may indicate failure to attain equilibrium (but see following discussion for alternative explanations). A similar gap appears in previous studies (Fig. 1), with no chloritoid compositions falling between $X_{Fe} = 0.88$ to 0.92. Because this compositional gap appears in data from

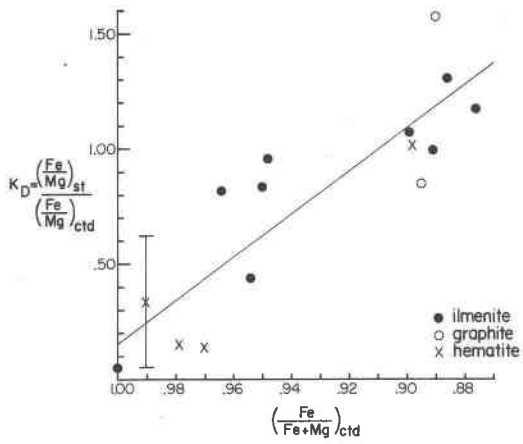

Fig. 10. Variation in K_D (Fe–Mg, st-ctd) with chloritoid composition can be expressed as $K_D = -9.38 X_{Fe,ctd} + 9.53$, $r^2 = 0.74$. Samples are keyed to oxides (see Fig. 9) and maximum error in K_D is shown. Errors in $X_{Fe,ctd}$ are less than ± 0.006, roughly the size of symbols. Notice the lack of chloritoid with X_{Fe} between 0.90 and 0.95. Sample P26e is not shown.

different studies, in different geographic locations, it too seems to be part of the natural phase relations of the two minerals.

Causes of Fe–Mg reversals

Possible causes of the Fe–Mg reversals, and of trends shown in Figure 10, can be identified by considering the form of the distribution coefficient K_D for the Fe–Mg exchange reaction

$$\text{Fe chloritoid} + \text{Mg staurolite} = \text{Mg chloritoid} + \text{Fe staurolite}. \quad (1)$$

This distribution coefficient K_D is

$$K_D = \frac{(X_{Mg,ctd})\,(X_{Fe,st})}{(X_{Fe,ctd})\,(X_{Mg,st})}. \quad (2)$$

If Fe and Mg were to mix on a single crystallographic site in each mineral; if all Mg were exchangeable for Fe; and if the two cations were to mix ideally, then K_D would equal the equilibrium constant for exchange Reaction (1). Because K_D varies with X_{Fe} at constant P and T (Fig. 10), it cannot be a valid measurement of the equilibrium constant for reaction (1); hence, one of the above assumptions must be violated. Thus there are three possible explanations for the observed Fe–Mg reversal: (1) Fe and Mg occupy more than one symmetrically distinct crystallographic site in staurolite and/or in chloritoid; (2) some Mg or Fe is not exchangeable in one phase; or (3) Fe and Mg do not mix ideally in one or both minerals. The three explanations have different petrologic consequences, and each explanation is consistent with available data.

Multiple site hypothesis

If Fe and Mg mix ideally on each individual site but occur on several symmetrically distinct sites in one or both minerals, then Fe/Mg ratios for that mineral may vary from site to site. Given such a situation, microprobe Fe/Mg values cannot be used directly in considering Fe–Mg partitioning. This type of relationship is well known in the system clinopyroxene–orthopyroxene (see Grover and Orville, 1969; and Kretz, 1981, p. 494–495 for a recent review of pertinent literature), and it may apply to chloritoid–staurolite as well.

It seems likely that Fe and Mg mix on a single site in chloritoid, because the chloritoid structure accepts divalent cations only in octahedral sites (Halferdahl, 1961; Hanscom, 1975, 1980). However, Fe–Mg mixing may not be ideal. Site occupancies are considerably more complicated in staurolite. Staurolite contains Fe in a tetrahedral site (designated Fe^{IV}) but Mössbauer spectra show that only about 75 percent of the Fe occupies this site (Smith, 1968). X-ray studies are unable to resolve which sites are filled by the remainder of the Fe, but Smith (1968) suggested that Fe might occupy two partially filled octahedral sites and might also substitute for Al in two additional octahedral sites (all designated Al^{VI}). Smith was unable to determine the site occupancy of Mg. Griffen and Ribbe (1973), based on principal component analysis of staurolite, suggested that major substitutions were Fe = (Zn,Al) in the Fe^{IV} site and Al = (Fe,Mg) in the Al^{VI} site. Therefore Fe and Mg may occupy several types of symmetrically distinct sites in staurolite.

Assuming a simplified case, that Fe and Mg mix ideally on one site in chloritoid and on two sites in staurolite, effects of multiple site mixing on K_D can be considered. For staurolite, measured values of Fe/(Fe+Mg) represent:

$$X_{Fe} = \frac{n_1 X_{Fe,1,St} + n_2 X_{Fe,2,St}}{n_1 + n_2}$$

where X_{Fe} = Fe/(Fe+Mg) in the mineral analysis, n_1 and n_2 are the number of sites of types 1 (Fe^{IV}) and 2 (Al^{VI}) respectively, that are occupied by Fe and Mg, and $X_{Fe,1,St}$ and $X_{Fe,2,St}$ refer to sites 1 and 2 of staurolite. The distribution coefficient K_D thus measures

$$K_D = \frac{X_{Mg,ctd}(n_1 X_{Fe,1,St} + n_2 X_{Fe,2,St})}{X_{Fe,ctd}(n_1 X_{Mg,1,St} + n_2 X_{Mg,2,St})} \quad (3)$$

which can differ significantly from the equilibrium constant for the Fe–Mg exchange Reaction (4),

$$\text{Fe ctd} + \left(\frac{n_1}{n_1 + n_2}\right)\text{Mg,1,St} + \left(\frac{n_2}{n_1 + n_2}\right)\text{Mg,2,St} = \text{Mg ctd} + \left(\frac{n_1}{n_1 + n_2}\right)\text{Fe,1,St} + \left(\frac{n_2}{n_1 + n_2}\right)\text{Fe,2,St}. \quad (4)$$

The equilibrium constant for Reaction (4) is

$$K_4 = \frac{X_{Mg,ctd}}{X_{Fe,ctd}}\left(\frac{X_{Fe,1,St}}{X_{Mg,1,St}}\right)^{n_1/(n_1+n_2)}\left(\frac{X_{Fe,2,St}}{X_{Mg,2,St}}\right)^{n_2/(n_1+n_2)}, \quad (5)$$

when mixing occurs on two sites in staurolite, given the site occupancy constraints outlined above. Although realistic appraisals of Equation (5) are impossible unless precise site occupancies of staurolite are known, the equation shows that a reversal in K_D does not necessarily require a reversal in K_4 (*cf.* Grover and Orville, 1969; Kretz, 1981).

Incomplete exchangeability of Fe and Mg

A second possibility suggested by the complex site occupancy of staurolite (Smith, 1968; Hollister, 1970; Griffen and Ribbe, 1973) is that some Mg may not be exchangeable with Fe in staurolite. This could be related to coupled substitutions that introduce trace amounts of Mg but not Fe into the staurolite structure. Such substitutions were suggested by Hollister (1970) based on microprobe analyses of sector-zoned staurolites. Hollister proposed substitutions of the type Ti + Mg = 2Al, and more

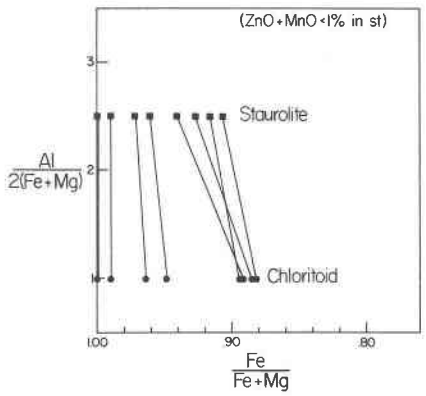

Fig. 11. AFM projection (Thompson, 1957) showing compositions of chloritoid and staurolite, with 0.13 weight percent MgO subtracted from staurolite (see text). Such subtraction eliminates the Fe–Mg reversal, suggesting the possibility that the reversal is caused by traces of Mg that are not exchangeable with Fe in staurolite.

complex substitutions involving Ti, with Fe not participating in the substitutions. If as little as 0.13 wt.% MgO is not exchangeable with FeO, equivalent to 0.05 atoms of Mg per formula unit and reducing exchangeable Fe/(Fe+Mg) by 0.01 to 0.02 in staurolite, the apparent Fe–Mg reversal disappears (Fig. 11). The only exceptions occur in several zincian samples.

Variation plots do not show any relationship between Mg and Ti in staurolite (Fig. 12d), but this does not disprove the possibility of coupled Mg + Ti substitutions. All analyzed staurolite crystals have at least 0.05 atoms of Ti per formula unit, enough Ti to account for the Fe–Mg reversal if all Ti were linked to Mg.

Substitution diagrams do show several other trends in these staurolites. There is a negative correlation between Al and Si ($r^2 = 0.31$, Fig. 12a) suggesting substitutions of the type $3Si^{4+} = 4Al^{3+}$. However, the total variation in Si is only half the total variation in Al, so Al must be substituting for constituents besides Si in the staurolite structure. There is a strong negative correlation between Al and total divalent cations ($r^2 = 0.66$, Fig. 12b), indicating substitutions between these constituents. Plots of Fe or Mg against Al also show negative slopes but have considerably more scatter ($r^2 = 0.26$, 0.40) than total divalent cations against Al, suggesting that Al substitutes for all divalent cations rather than just one. If this inference is correct, then these substitutions are unrelated to the Fe–Mg reversal.

The slope of the least-squares line to a plot of Al *vs.* total divalent cations in staurolite (Fig. 12b) has a slope of −1.00 rather than the value of −1.50 expected from charge-balance considerations. This probably indicates a coupled substitution rather than simple Al = Fe exchange. There is no significant relationship between Si and total divalent cations, with linear regression yielding r^2 of 0.005 (Fig. 12c), so Si does not seem to be involved in this coupled substitution. The data could be explained by variable H^+ content of staurolite, with substitutions such as $Al^{3+} = Fe^{2+} + H^+$; recent work has shown that staurolite can have variable H^+ (S. L. Lonker, pers. comm.).

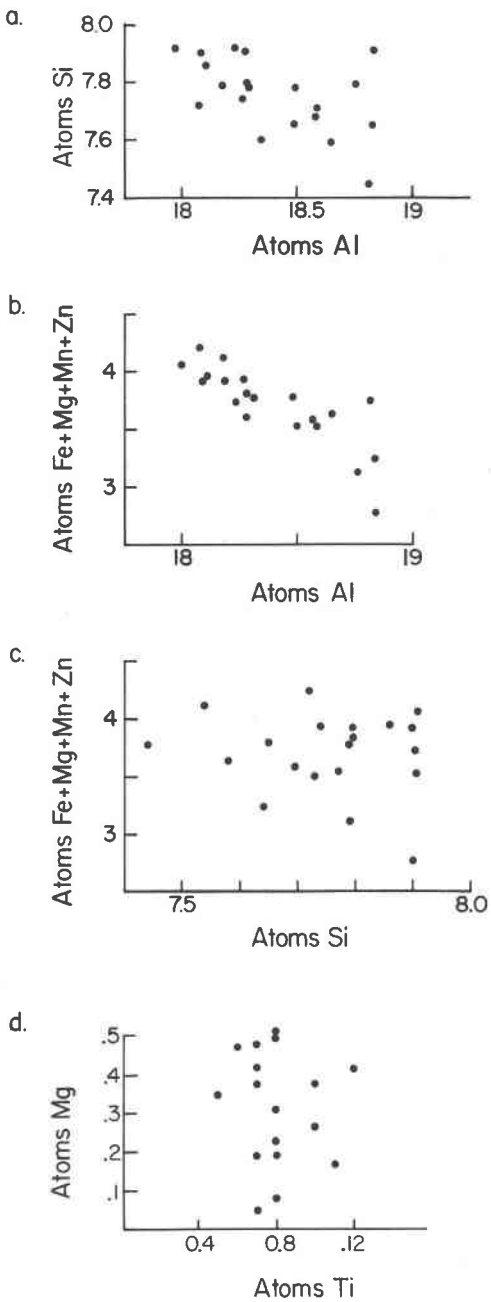

Fig. 12. Compositional variations in staurolite compiled from Table 5. Least-squares fits to the data yield: (a) Si = −0.25 Al + 12.45, $r^2 = 0.31$; (b) total divalent cations = −1.00 Al + 22.15, $r^2 = 0.66$; (c) total divalent cations = −100 Si + 780, $r^2 = 0.005$; (d) Ti = −0.04 Mg + 0.10, $r^2 = 0.11$.

Non-ideal mixing of Fe and Mg

If the distribution coefficient K_D reflects mixing on a single site, with total exchangeability of Fe and Mg, then Fe–Mg mixing must be non-ideal: ideal solution precludes dependence of K_D on mineral Fe/(Fe+Mg) ratios. Given non-ideal mixing, the equilibrium constant for exchange Reaction (1) can be rewritten as

$$K_1 = \frac{(\gamma_{Mg,ctd}X_{Mg,ctd})\,(\gamma_{Fe,st}X_{Fe,st})}{(\gamma_{Fe,ctd}X_{Fe,ctd})\,(\gamma_{Mg,st}X_{Mg,st})} \qquad (6)$$

where γ refers to activity coefficients for the end-member compositions in each mineral. To create the trend seen in Figure 10, activity coefficients must vary with mineral composition.

Non-ideal mixing of Fe and Mg might be expected on the Fe^{IV} site of staurolite, based on crystal-chemical considerations. Volumetric data indicate that Fe–Mg mixing may indeed depart from ideality: relationships between molar volume and X_{Fe} depart notably from a linear trend in staurolite (Schreyer and Seifert, 1969, Fig. 2).

Chloritoid may also depart from an ideal Fe–Mg solution. Two points support this: (1) although staurolite and garnet show a continuum of compositions, chloritoid shows a distinct gap if data from sample P26e are ignored (Fig. 1). This gap might represent a solvus, or at least a strong departure from ideal Fe–Mg mixing. (2) Sample P26e may represent a disequilibrium assemblage, but it seems unlikely that the only sample with zoned chloritoid would plot within the gap in X_{Fe} shown by other samples. An alternative explanation is that P26e does contain an equilibrium assemblage, but chloritoid shows positive excess free energy of Fe–Mg mixing. To explain the chemical complexities of P26e, analogy may be drawn to the distribution of K and Na between alkali feldspar and vapor (Orville, 1963). At supersolvus conditions, vapor of nearly constant composition (K/(Na+K) = 0.26) can coexist with feldspar having any composition between Or_{18} and Or_{31}. This occurs as a result of non-ideal K–Na mixing in feldspar near the albite–orthoclase solvus (Orville, 1963, Fig. 3). The result is a reversal in distribution of K and Na between feldspar and vapor. Analogy to chloritoid–staurolite would suggest that, if sample P26e represents equilibrium, staurolite of composition X_{Fe} = 0.93 can coexist with chloritoid having any composition between X_{Fe} = 0.90 and 0.95. If the Fe–Mg reversal is due to non-ideality of Fe–Mg exchange in chloritoid, chloritoid might show a true solvus at lower temperatures.

Implications of Fe–Mg reversals

Consequences of the Fe–Mg reversal are best examined by their effects on a simple mineral reaction such as

$$2\ \text{ctd} + 5\ \text{ky} = 1\ \text{st} + 1\ \text{qtz} + 3\ H_2O. \qquad (7)$$

In an isobaric T–X_{Fe} plot, the form of Reaction (7) is critically dependent on the actual cause of the Fe–Mg reversal. If the reversal is caused by incompletely exchangeable Fe and Mg in staurolite, then staurolite is uniformly higher in X_{Fe} than chloritoid when only exchangeable cations are considered (Fig. 11). If the reversal is caused by mixing on multiple sites in staurolite, it is also likely that staurolite has higher "effective" X_{Fe} than chloritoid. Therefore both possibilities predict that Reaction (7) should proceed at lowest temperatures for Fe end member compositions, that experiments of Richardson (1968) and Ganguly (1972, 1977) define the minimum thermal stability of staurolite + quartz in the Fe–Mg system, and that the widely accepted AFM topologies and reaction sequences of Albee (1972) are valid.

Alternatively, if the reversal is caused by non-ideal mixing of Fe and Mg in either mineral, then petrologic implications are significantly different. Reaction (7) should show an extremal state with composition near X_{Fe} = 0.909 (Korzhinskii, 1966; *cf.* Korikovskii, 1969, who inferred an extremal state for chloritoid–staurolite–garnet near $X_{Fe,ctd}$ = 0.907). Non-ideal mixing would require a minimum in the T–X_{Fe} loop for reaction (7) at X_{Fe} = 0.909 (Fig. 13), suggesting that experimental studies in the Fe end-member system do not define the minimum stability temperature of staurolite + quartz in the Fe–Mg system.

If the Fe–Mg reversal is caused by non-ideal Fe–Mg mixing in chloritoid, then all data presented in this study can be explained easily, including the gap in chloritoid compositions (Fig. 1) and the complex zoning of chloritoid in specimen P26e (Fig. 4). However, no evidence directly contradicts the other possible causes of the Fe–Mg reversal.

Conclusions

Fifteen specimens of metamorphic rock from the Truchas Range, and several samples from the nearby Picuris Range, contain coexisting chloritoid and staurolite. Fe–

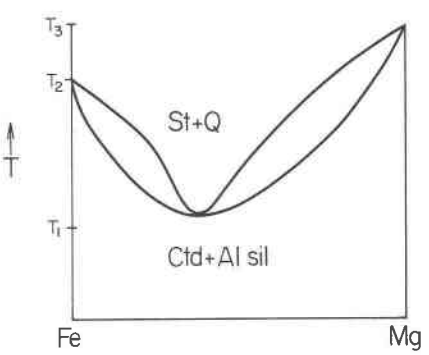

Fig. 13. Pseudo-bivariant T–X_{Fe} loop for reaction (8), showing topology required if the Fe–Mg reversal is caused by non-ideal mixing of the two cations. The minimum in the loop should occur near X_{Fe} = 0.909. The differences in temperature between T_1 and T_2, and between T_2 and T_3, cannot be calculated without knowing the mixing properties of Fe and Mg in both minerals.

Mg distribution coefficients ($K_{D,ctd\text{-}st}$) vary inversely with chloritoid composition, following a trend expressed as $K_D = -9.38\ X_{Fe,ctd} + 9.53$ ($r^2 = 0.74$, Fig. 10). The two minerals show a reversal in Fe–Mg partitioning at $X_{Fe} = 0.909 \pm 0.019$. This reversal seems to be part of the equilibrium phase relations between the minerals and might be caused by any of three factors: (1) Fe and Mg may mix on several symmetrically distinct sites in one mineral; (2) some Mg may not be exchangeable with Fe in one mineral, probably staurolite; or (3) Fe and Mg may mix non-ideally in one or both phases. Any combination of two or more factors could also cause the observed Fe–Mg reversal.

The significance of the reversal depends largely on its cause. Possibilities (1) and (2) suggest that experiments of Richardson (1968) and Ganguly (1972, 1977) define the minimum stability temperature of staurolite + quartz in the system $FeO–MgO–Al_2O_3–SiO_2–H_2O$. Possibility (3) suggests otherwise; it indicates that the reaction producing staurolite + quartz in metamorphic rocks should proceed at its lowest temperature near $X_{Fe} = 0.909$.

There are two ways to test the three proposed causes of the Fe–Mg reversal. The first would involve detailed crystallographic analyses of chloritoid and staurolite, yielding precise information about site occupancies of Fe and Mg in each phase. Previous investigators (Smith, 1968; Griffen and Ribbe, 1973) have not had success with this approach with staurolite, but it has not been tried with chloritoid. Perhaps refined experimental techniques such as extended X-ray absorption, fine-structure spectroscopy (EXAFS; Sandstrom and Lytle, 1979) could provide definitive information on site occupancy in staurolite. Alternatively, a second test might involve experimental studies, either on the T–X_{Fe} stability of chloritoid + Al silicate (*cf.* Fig. 13), or on calorimetric properties of Fe–Mg chloritoid.

Acknowledgments

I thank D. B. Codding for separating minerals for chemical and X-ray analysis, M. J. Holdaway for providing samples from the Picuris Range, J. Husler for performing wet chemical analyses, and G. Carnako for assistance in translating portions of Korikovskii (1969) from the Russian. The manuscript was improved significantly by critical reviews of D. A. Hewitt, L. S. Hollister and C. J. Yapp. Research was supported by Sandia National Laboratories and by NSF grant EAR-8115530.

References

Albee, A. L. (1972) Metamorphism of pelitic schists: reaction relations of chloritoid and staurolite. Geological Society of American Bulletin, 83, 3249–3278.

Alder, H. L. and Roessler, E. B. (1972) Introduction to probability and statistics. San Francisco, W. H. Freeman.

Baltatzis, E. (1979) Staurolite-forming reactions in the eastern Dalradian rocks of Scotland. Contributions to Mineralogy and Petrology, 69, 193–200.

Bence, A. E. and Albee, A. L. (1968) Empirical correction factors for the electron microanalysis of silicates and oxides. Journal of Geology, 76, 382–403.

Ferry, J. M. and Spear, F. S. (1978) Experimental calibration of the partitioning of Fe and Mg between biotite and garnet. Contributions to Mineralogy and Petrology, 66, 113–117.

Fox, J. S. (1971) Coexisting chloritoid and staurolite and the staurolite–chlorite isograd from the Agnew Lake area, Ontario, Canada. Geological Magazine, 108, 205–219.

Ganguly, J. (1972) Staurolite stability and related parageneses: theory, experiments, and applications. Journal of Petrology, 13, 335–365.

Ganguly, J. (1977) Compositional variables and chemical equilibrium in metamorphism. In S. K. Saxena and S. Bhattacharji, Eds., Energetics of Geological Processes, p. 250–284. Springer-Verlag, New York.

Grambling, J. A. (1979) Precambrian geology of the Truchas Peaks region, north-central New Mexico, and some regional implications. New Mexico Geological Society Guidebook 30, 135–143.

Grambling, J. A. (1981) Kyanite, andalusite, sillimanite, and related mineral assemblages in the Truchas Peaks region, New Mexico. American Mineralogist, 66, 702–722.

Greenwood, H. J. (1975) Thermodynamically valid projections of extensive phase relationships. American Mineralogist, 60, 1–8.

Gresens, R. L. (1975) Geochronology of Precambrian metamorphic rocks, north-central New Mexico. Geological Society of America Bulletin, 87, 1444–1448.

Griffen, D. T. and Ribbe, P. H. (1973) The crystal chemistry of staurolite. American Journal of Science, 272A, 479–495.

Grover, J. E. and Orville, P. M. (1969) The partitioning of cations between coexisting single and multi-site phases with application to the assemblages: orthopyroxene–clinopyroxene and orthopyroxene–olivine. Geochimica et Cosmochimica Acta, 33, 205–226.

Halferdahl, L. B. (1961) Chloritoid: its composition, x-ray and optical properties, stability, and occurrence. Journal of Petrology, 2, 49–135.

Hanscom, R. H. (1975) Refinement of the crystal structure of monoclinic chloritoid. Acta Crystallographica, B 31, 780–784.

Hanscom, R. H. (1980) The structure of triclinic chloritoid and chloritoid polytypism. American Mineralogist, 65, 534–539.

Holcombe, R. J. and Callender, J. F. (1982) Structural analysis and stratigraphic problems of Precambrian rocks of the Picuris Range, New Mexico. Geological Society of America Bulletin, 93, 138–149.

Holdaway, M. J. (1978) Significance of chloritoid-bearing rocks in the Picuris Range, New Mexico. Geological Society of America Bulletin, 89, 1404–1414.

Holdaway, M. J. and Lee, S. M. (1977) Fe–Mg cordierite stability in high-grade pelitic rocks based on experimental, theoretical and natural observations. Contributions to Mineralogy and Petrology, 63, 175–198.

Hollister, L. S. (1969) Contact metamorphism in the Kwoiek area of British Columbia: an end member of the metamorphic process. Geological Society of America Bulletin, 80, 2465–2494.

Hollister, L. S. (1970) Origin, mechanism and consequences of compositional sector-zoning in staurolite. American Mineralogist, 55, 742–766.

Kepezhinskas, K. B. and Khlestov, V. V. (1977) The petrogenetic grid and subfacies for middle-temperature metapelites. Journal of Petrology, 18, 114–143.

Korikovskii, S. P. (1969) Phase equilibria in low-temperature part of staurolitic facies under the conditions of different depths. Akademiaa Nauk SSSR, Izvhestia Seriaa Geographica, 8, 40–56.

Korzhinskii, D. S. (1966) Extreme conditions and their significance in mineral systems. In A. P. Vinogradov, Ed., Chemistry of the Earth's Crust, v. 1, Academy of Sciences of the USSR (English translation, N. Kaner and R. Amoils, Israel Program for Scientific Translations).

Kretz, R. (1981) Site-occupancy interpretation of the distribution of Mg and Fe between orthopyroxene and clinopyroxene in metamorphic rocks. Canadian Mineralogist, 19, 493–500.

Labotka, T. C., Papike, J. J., Vaniman, D. T. and Morey, G. B. (1981) Petrology of contact metamorphosed argillite from the Rove Formation, Gunflint Trail, Minnesota. American Mineralogist, 66, 70–86.

Lal, R. K. and Ackermand, D. (1979) Coexisting chloritoid–staurolite from the sillimanite (fibrolite) zone, Sini, district Singhbhum, India. Lithos, 12, 133–142.

Long, L. E. (1972) Rb–Sr chronology of Precambrian schist and pegmatite, La Madera Quadrangle, northern New Mexico. Geological Society of America Bulletin, 83, 3425–3432.

Montgomery, Arthur (1953) Precambrian geology of the Picuris Range, north-central New Mexico. New Mexico Bureau of Mines and Mineral Resources, Bulletin 30.

Montgomery, Arthur (1963) Precambrian rocks. In J. P. Miller, Arthur Montgomery, and P. K. Sutherland, Geology of part of the southern Sangre de Cristo Mountains, New Mexico. New Mexico Bureau of Mines and Mineral Resources, Memoir 11.

Orville, P. M. (1963) Alkali ion exchange between vapor and feldspar phases. American Journal of Science, 261, 201–237.

Richardson, S. W. (1968) Staurolite stability in a part of the system Fe–Al–Si–O–H. Journal of Petrology, 9, 467–488.

Rumble, D. III (1971) Chloritoid–staurolite quartzites from the Moosilauke quadrangle, New Hampshire. Carnegie Institute of Washington, Yearbook 69, 290–294.

Rumble, D. III (1978) Mineralogy, petrology and oxygen isotopic geochemistry of the Clough Formation, Black Mountain, western New Hampshire, U.S.A. Journal of Petrology, 19, 317–340.

Sandstrom, D. R. and Lytle, F. W. (1979) Developments in extended X-ray absorption fine structure applied to chemical systems. Annual Review of Physics and Chemistry, 30, 215–238.

Schreyer, W. and Seifert, F. (1969) High-pressure phases in the system $MgO–Al_2O_3–SiO_2–H_2O$. American Journal of Science, 267A, 407–443.

Smith, J. V. (1968) The crystal structure of staurolite. American Mineralogist, 53, 1139–1155.

Thompson, A. B. (1976) Mineral reactions in pelitic rocks: II. Calculations of some P–T–X(Fe–Mg) phase relations. American Journal of Science, 276, 424–454.

Thompson, J. B. Jr. (1957) The graphical analysis of mineral assemblages in pelitic schists. American Mineralogist, 42, 842–858.

Tracy, R. J., Robinson, P. and Thompson, A. B. (1976) Garnet composition and zoning in the determination of temperature and pressure of metamorphism, central Massachusetts. American Mineralogist, 61, 762–775.

Manuscript received, April 6, 1982;
accepted for publication, November 15, 1982.